Homogeneous Dislocation-Induced Rainbow Concentrating for Elastic Waves

Zi-Dong Zhang,[1,‡] Shi-Li Yang,[1,‡] Shi-Ling Yan,[1] Si-Yuan Yu,[1,2,*] Ming-Hui Lu,[1,2,†] and Yan-Feng Chen[1,2]

[1] *National Laboratory of Solid State Microstructures & Department of Materials Science and Engineering, Nanjing University, Nanjing 210093, China*

[2] *Jiangsu Key Laboratory of Artificial Functional Materials, Nanjing University, Nanjing 210093, China*

(Received 11 May 2022; accepted 1 September 2022; published 6 October 2022)

Defects play a crucial role in the physical properties of crystals, whether for classical or quantum systems. For example, in photonic and phononic crystals, defects can serve as precise guidance for and localization of classical electromagnetic or mechanical waves. Rainbow concentrating, an exotic wave localization, exploits defects to enable the collection and frequency routing of weak signals in real space. Here, using a solid-state phononic crystal (PnC) plate, we experimentally verify this phenomenon by deliberately infusing a homogeneously graded dislocation, i.e., a line defect, into the PnC. Two PnCs separated by the defect will breed deterministic interface states along with the defect, offering rainbow trapping and concentrating for elastic waves. Our PnC-based rainbow trappers and concentrators are scalable and configurable, and thus, are promising for advancing applications like energy harvesting, information processing, and acoustofluidic manipulation.

DOI: 10.1103/PhysRevApplied.18.044015

I. INTRODUCTION

Accurately guiding and trapping waves, whether in electromagnetics [1–3] or mechanics [4–12], lie at the heart of artificial microstructures and metamaterials and are crucial for realizing applications, e.g., sensing, energy harvesting [13], and information processing [14]. For periodic microstructures, such as photonic crystals (PCs) and phononic crystals (PnCs), the introduction of defects into the crystals can bring about defect modes, which can be used to guide and trap those classical waves. Since the frequencies of these defect modes are closely related to the defects themselves, if a crystal has spatially continuous and graded defects, they can be used to distribute waves of different frequencies to different locations in real space, i.e., rainbow trapping [15]. For electromagnetic waves and airborne sounds, rainbow trapping is well observed in both one-dimensional (1D) and two-dimensional (2D) systems [16–24]. For a 1D (chainlike) elastic system, rainbow trapping is achieved by band-structure engineering based on chirped PnCs [25], an elastic waveguide loaded with an array of resonators [26–29], and a graded piezoelectric metamaterial beam [30]. For the 2D (platelike) elastic system, however, the development of this effect or function is lagging behind. In a 2D elastic system, despite few proposed rainbow trappers, these solutions require relatively complex technical means (either manipulating the thickness of the plate [31] or the height of the column resonators [32]), which brings great difficulties for sample preparation in continuous elastic media. In 2020, Nakata *et al*. devised a scheme that produced a series of zero-dimensional localized states in a defect created by a translational deformation of a periodic potential [33]. This scheme allows frequency modulation of defect modes simply by translating the microstructures, undoubtedly providing a convenient and feasible path for 2D elastic rainbow phenomena. This method has recently been extended theoretically to electromagnetic waves [34]. Lu *et al*. demonstrated the rainbow trapper and further rainbow concentrator by region-selectively introducing translation into nanostructures in a PC. The so-called rainbow concentrator is an extension of the rainbow trapper. It greatly expands the working direction of the latter, from unidirectional to multidirectional, which is more efficient and conducive to practical applications.

Here, based on a 2D PnC plate, we experimentally realize both elastic rainbow trapping and concentrating. By infusing a homogeneous dislocation, i.e., a line defect, into the PnC, two separated PnCs will have distinct Zak phases, leading to deterministic interface states along with the defect. Different translations can modulate the group velocity of these interface states, offering the verification of rainbow trapping and concentrating for elastic waves. All these PnC-based rainbow trappers and concentrators

*yusiyuan@nju.edu.cn
†luminghui@nju.edu.cn
‡Z.-D. Zhang and S.-L. Yang contributed equally to this work.

are convenient to design and configurable. By setting different degrees of defect gradient, both mode volume and frequency spacing of adjacent rainbow modes are adjustable.

II. ELASTIC DETERMINISTIC INTERFACE STATES ON A HOMOGENEOUS DISLOCATION

Our elastic rainbow PnC is designed from a plate with mounted columns in a 2D square lattice, as illustrated in Fig. 1(a). The unit cell of the PnC is a square plate with identical square columns on both sides, placed in the center of the cell. In this study, the PnC is made from aluminum alloy for demonstration. Its lattice constant, a, is 2 cm. The plate thickness, d; the height of the square columns, H; and their lateral size, b, equal $0.4a$, $0.35a$, and $0.5a$, respectively.

If the columns are only mounted on one side of the plate, the plate's mirror symmetry along its center plane will be broken, leading to ubiquitous hybridization of the extensional and shear-horizontal (SH) modes and out-of-plane flexural modes. For the convenience of this study, we choose to have the same columns on both sides of the plate. In this plate PnC, the pure out-of-plane modes are now independent (decoupled) from the others [35]. In most scenarios, the two types of modes cannot be converted into each other, so they can be studied and exploited separately.

Figure 1(b) shows the calculated band structure of this plate PnC, with the inset corresponding to its Brillouin zone. By calculating a polarization index, the two types of modes are well distinguished (see Supplemental Material Note 1 [36]). Here, we choose only one of them for experimental demonstration [i.e., the modes with out-of-plane components (specifically, flexural modes)]; in fact, the design scheme for both of them is almost the same. The band structure shows that the flexural modes have a full band gap from about 58 to 80 kHz in our plate PnC.

Next, we apply a 2D translation vector $\xi = (\xi_x, \xi_y)$ to all the columns of the PnC, parallel to the plate surface. This translation vector can be regarded as a synthetic dimension, which, together with the Bloch wave vector, $\mathbf{k} = (k_x, k_y)$, forms a four-dimensional parameter space (ξ_x, ξ_y, k_x, k_y). Because the four parameters are all periodic, the

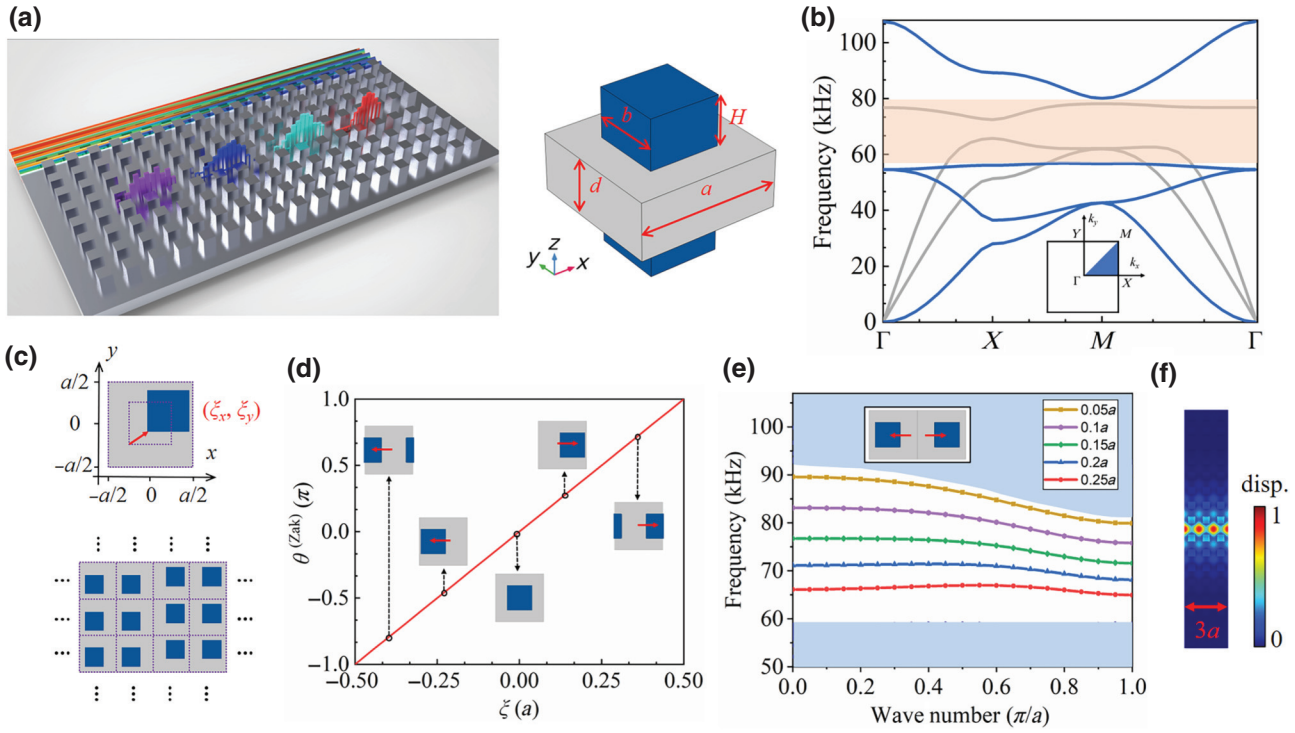

FIG. 1. Elastic deterministic interface states on a homogeneous dislocation. (a) Schematic of our 2D elastic rainbow PnC, with identical columns on both sides of a plate. Enlarged view shows its unit cell in a square lattice. (b) Calculated 2D band structure. Blue (gray) lines correspond to the out-of-plane flexural modes (extensional and SH modes). Inset is the Brillouin zone. (c) Domain-boundary formation by applying a 2D translation vector, $\boldsymbol{\xi}$, to different parts of the PnC. (d) Zak-phase evolution as a function of ξ_x. (e) Band structures of the deterministic interface states on a homogeneous dislocation. Inset shows a schematic of the dislocation, where $\boldsymbol{\xi}_L = (\xi_x, \xi_y)$ and $\boldsymbol{\xi}_R = (-\xi_x, \xi_y)$. Blue shaded regions are bulk bands. (f) Calculated out-of-plane-displacement field distribution of an interface state ($\xi_x = 0.1a$, $k = 1$).

periodic gauge can be imposed on eigenstates, which is

$$\begin{aligned}|\psi_n(\xi_x + a, \xi_y, k_x, k_y)\rangle &= |\psi_n(\xi_x, \xi_y + a, k_x, k_y)\rangle,\\ &= |\psi_n(\xi_x, \xi_y, k_x + 2\pi a, k_y)\rangle,\\ &= |\psi_n(k_x, \xi_y, k_x, k_y + 2\pi a)\rangle,\\ &= |\psi_n(\xi_x, \xi_y, k_x, k_y)\rangle,\end{aligned}$$

where $|\psi_n(\xi_x, \xi_y, k_x, k_y)\rangle$ denotes the eigen Bloch state with parameter (ξ_x, ξ_y, k_x, k_y) and band number n. If we spatially divide the 2D PnC into two continuous parts and apply different translation vectors to them, two domains will be formed in this PnC, accompanied by the appearance of a 1D domain boundary.

As shown in Fig. 1(c), we divide the 2D PnC into two parts along the y direction and apply translation vectors $\boldsymbol{\xi}_L$ and $\boldsymbol{\xi}_R$ to the left and right halves, respectively. In this way, we construct a domain boundary along the y direction in the PnC. Since this domain boundary is straight and parallel to the high-symmetry direction of the PnC, such a 2D PnC can be equivalently reduced to 1D, and the 1D domain boundary can be equivalently reduced to zero dimensional (0D). For 1D PCs and PnCs containing different domains, the topological properties of 0D boundaries can be investigated by examining the Zak phases of the domains [37,38]. This method also works for our system. Figure 1(d) shows the Zak phases of our PnC as a function of ξ_x (keeping ξ_y constant). When ξ_x changes from $-0.5a$ to $0.5a$, the Zak phase increases continuously from $-\pi$ to π [36]. Note that whatever ξ_x is introduced, the PnC's band structure remains the same.

The Zak-phase distinction between two domains guarantees deterministic interface states, as proven extensively in electromagnetic [39–45] and mechanical systems [46]. In our PnC, we introduce a homogeneous dislocation [47] to achieve this Zak-phase distinction. Specifically, the x (y) components of the translation vector of the two domains are set to negative (consistent), i.e., $\boldsymbol{\xi}_L = (\xi_x, \xi_y)$ and $\boldsymbol{\xi}_R = (-\xi_x, \xi_y)$. Also, to avoid damaging the integrity of the column structure, the value of ξ_x is set to $0.25a$. This method greatly reduces the difficulty of sample preparation (see Supplemental Material Note 3 [36]). With this scheme, we successfully construct the deterministic interface states, as their band structures are shown in Fig. 1(e). The calculated displacement field distribution of one representative interface state is shown in Fig. 1(f), confirming that the elastic energy is mainly localized in the domain boundary, i.e., the homogeneous dislocation.

Note that these interface states are submerged into the bulk when there is no complete band gap (see Supplemental Material Note 4 [36]). Moreover, if the y (x) components of the translation vector of the two domains are set to negative (consistent), i.e., $\boldsymbol{\xi}_L = (\xi_x, \xi_y)$ and $\boldsymbol{\xi}_R = (\xi_x, -\xi_y)$, no interface states can be constructed (see Fig. S5 within the Supplemental Material [36]).

III. MODULATION OF THE INTERFACE STATES BY THE TRANSLATIONAL VECTOR $\boldsymbol{\xi}$

The interface states' operational bandwidth and group velocities can be tuned by the translational vector, $\boldsymbol{\xi}$. Figure 2(a) shows the interface states' group-velocity spectra under five different ξ_x. The group velocities are determined by $V_g = 2\pi\, df/dk$, derived from the calculated band structures [Fig. 1(e)]. All the spectra show a maximum value near the middle of their operation bandwidth. Also, at their frequency extrema (both minima and maxima), all group velocities become zero, owing to the differentiable nature of the phononic bands. To demonstrate the properties of boundary states more intuitively under different ξ_x, we also plot the group-velocity distribution as a function of continuous ξ_x, as shown in Fig. 2(b). Between 65 and 82 kHz (within the complete band gap of our PnC), as ξ_x increases from 0 to $0.25a$, both the maximum group velocity and the frequency extrema of the interface states decrease.

IV. ELASTIC RAINBOW TRAPPING THROUGH A GRADUALLY TUNED BOUNDARY

Rainbow trapping is a phenomenon in which states with different frequency components are dispersed and trapped at different spatial locations [22]. As mentioned above, since the frequency extrema of the elastic interface states

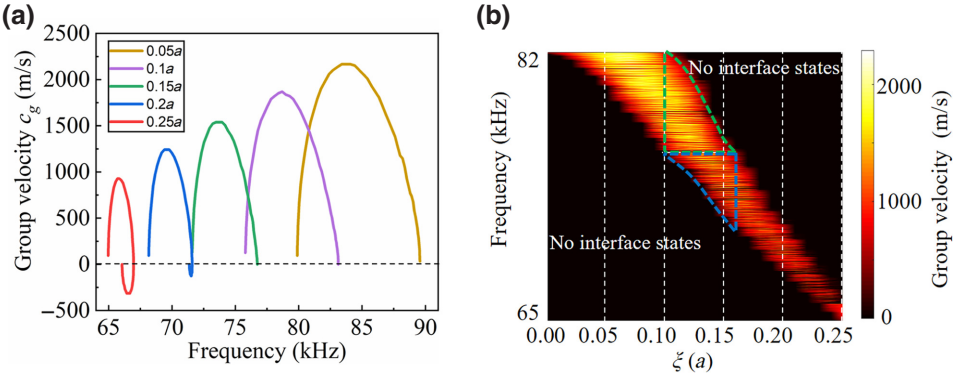

FIG. 2. Group velocity of interface states. (a) Group-velocity spectra of interface states when ξ_x equals $0.05a$, $0.1a$, $0.15a$, $0.2a$, and $0.25a$. (b) Group-velocity distribution with continuous variation of ξ_x. Bright region indicates interface states with a certain operation bandwidth; two dark regions represent the absence of interface states.

can be tuned via the geometrical translational vector, $\boldsymbol{\xi}$, and the group velocities at the extrema are always zero, these boundaries can therefore be utilized for rainbow trapping of elastic waves.

In the experiment, we fabricate a PnC containing one boundary with gradually tuned ξ_x from $0.1a$ to $0.16a$, as the sample shown in Fig. 3(a). An ultrasound piezoceramic transducer, acting as an elastic wave source, is placed at one port of the boundary. A scanning laser vibrometer is used to record the out-of-plane displacement of elastic waves near the boundary, working at different frequencies. The experimental scan area is indicated by the blue dashed box in Fig. 3(a), where ξ_x is from $0.105a$ to $0.1525a$. The results are shown in Fig. 3(b).

When the source is placed at the port where $\xi_x = 0.1a$, as the frequency increases, the distance the elastic waves travel along the boundary (and eventually stop, because of the zero group velocity) is reduced. In this case, since the near-source boundary ($\xi_x = 0.1a$) supports only elastic waves with frequencies from about 73.5 to 82 kHz, only waves in this frequency range can propagate along the boundary. As the wave propagates, ξ_x gets larger; thus, the supported frequency range gets narrower. For the elastic wave in lower frequency, e.g., 73.5 kHz, it can travel through the entire gradually tuned boundary. By contrast, the elastic wave in higher frequency, e.g., 78.5 kHz, can only travel a short distance before being forced to stop. The experimental results and analysis match the calculation in Fig. 2(b), which frames the rainbow-trapping frequencies (see the green region in the figure) for this scenario.

Rainbow trapping would be different if the source were placed at the port where $\xi_x = 0.16a$. In this case, since the near-source boundary ($\xi_x = 0.16a$) supports only elastic waves with frequencies from about 70 to 73.5 kHz, only waves in this frequency range can propagate along the boundary. Only the elastic wave in higher frequency, e.g., 73.2 kHz, can travel through the entire gradually tuned boundary. Simulation is performed for this scenario, as shown in Fig. 3(c), matching well with the calculation in Fig. 2(b) (see the blue region in the figure).

In both scenarios, when elastic waves of different frequencies are dispersed in the gradually tuned boundary, they will resonant where they stop, simply owing to their group velocity being reduced to zero at the location. Additionally, this elastic rainbow trapping applies not only to the flexural modes we demonstrate here but also to the in-plane modes. Within the complete in-plane-mode band gap, as shown in Fig. 1(c), our simulation validates that the in-plane modes can also be rainbow trapped by taking a similar approach (see Appendix A).

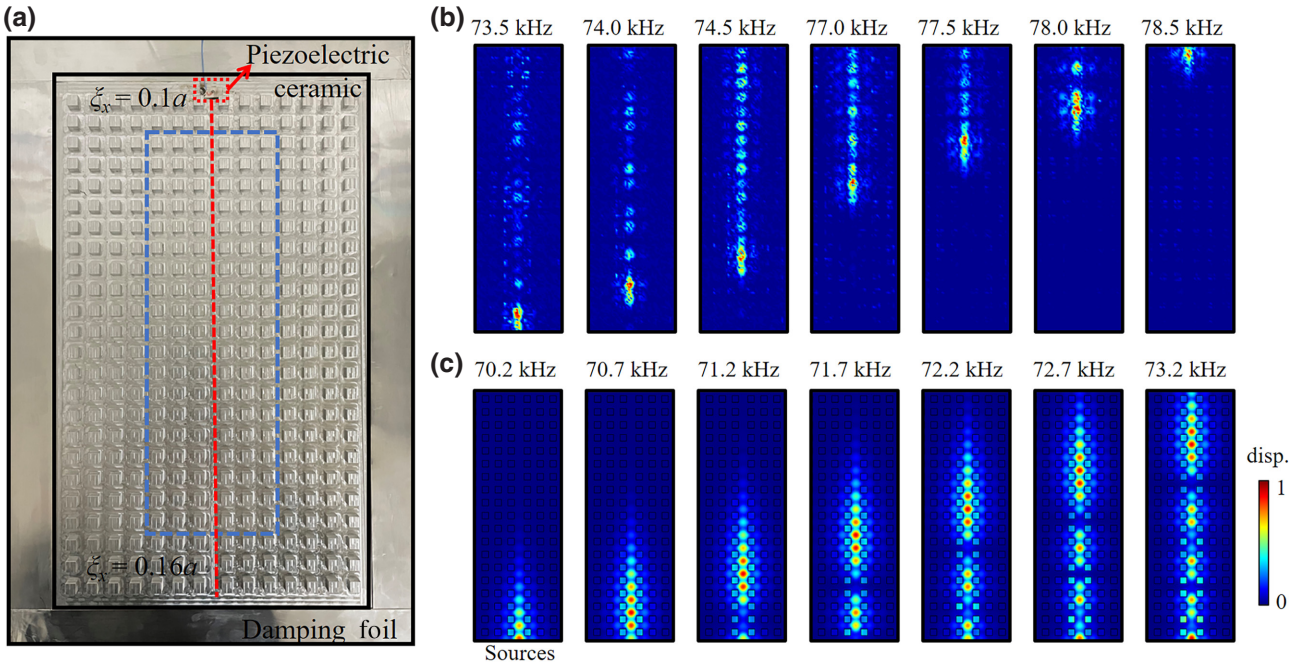

FIG. 3. Elastic rainbow trapping. (a) Photograph of our elastic PnC with a gradually tuned boundary. ξ_x equals $0.1a$ and $0.16a$ on the top and bottom ports of the boundary, respectively. PnC has 24 layers along the boundary direction, and the difference in ξ_x between each adjacent layer is $0.0025a$. Red dotted line marks the location of the rainbow waveguide. (b),(c) Out-of-plane-displacement field distributions in the PnC, when elastic waves of different frequencies enter the boundary from the top port (experimental results) and bottom port (simulated results), respectively.

V. ELASTIC RAINBOW CONCENTRATOR UTILIZING THE GRADUALLY TUNED BOUNDARY

As recently proposed [33], a rainbow concentrator can collect weak signals multidirectionally and assign different frequency components to different spatial locations. This effect can form a series of isolated rainbow resonant cavities in the band gap of phononic and photonic crystals, and their positions and frequencies (one-to-one correspondence) are all discrete. In all previous works, the position and frequency of acoustic rainbow resonance are continuous. Compared with traditional concentrators, e.g., in plasmonics [48] or transformation optics [49], which either operate over a narrow bandwidth or have no frequency resolution, a rainbow concentrator operates at multiple frequencies, and therefore, greatly improves the performance of a single device.

In the rainbow-trapping experiment, if we construct a boundary with ξ_x ranging from ξ_1 to ξ_2 ($\xi_1 < \xi_2$), elastic resonances of frequencies ranging from f_{ξ_2} to f_{ξ_1} may all be supported in the boundary but at different locations, where $f_{\xi_2}(f_{\xi_1})$ is the minimum (maximum) frequency of the boundary states in the case of ξ_2 (ξ_1). Since the elastic waves need to enter the boundary through the two ports (either one), this forces all ξ in the interval from the entrance port to the resonant position to support the resonant frequency (at the resonant position). However, if the elastic waves do not need to reach the resonant positions along the boundary, the operational bandwidth of the whole device will be greatly broadened. This idea also inspired us to realize an elastic rainbow concentrator and resonator.

Our proposed elastic rainbow concentrator is demonstrated using another PnC, containing one boundary with a more significant gradually tuned ξ_x from $0.06a$ to $0.22a$, as the sample shown in Fig. 4(a). In this PnC, there are only four layers of the columns on either side of the boundary. In the boundary direction, there are 33 layers, and $\Delta\xi_x$ between each adjacent layer is $0.005a$. The eigenvalue calculation in Fig. 4(b) shows that 28 resonant states exist in this PnC, which are continuously distributed at different boundary positions with a monotonic variation of frequency.

In this configuration, since the PnC is not thick enough to fully support its band gap, rainbow resonant states can be excited by elastic waves that do not propagate along the boundary. Experimentally, a row of ultrasound piezoceramic transducers, analogous to a plane-wave source for the elastic waves, is placed on the side of the PnC. Thus, the plane elastic waves pumped by the transducers are incident on the PnC perpendicular to the boundary direction. The scanning laser vibrometer records how the resonant modes are excited at different frequencies. Figure 4(c) shows the measured intensity spectrum of these resonant states when excited. Their resonant frequencies are

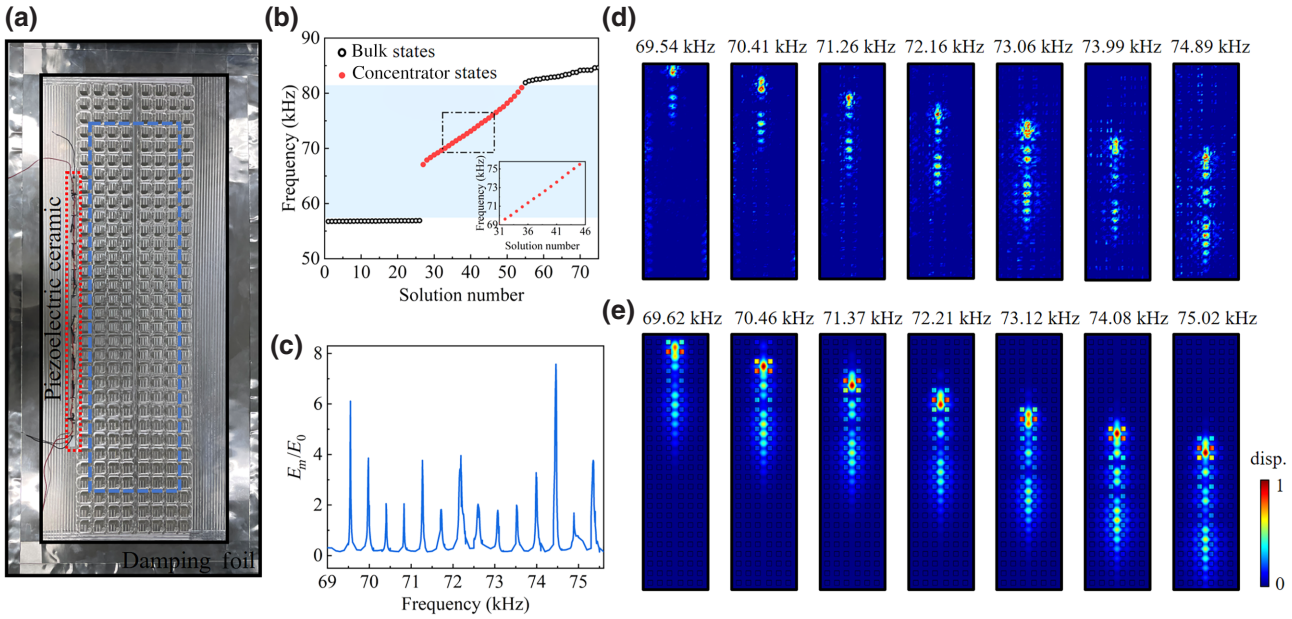

FIG. 4. Elastic rainbow concentrator. (a) Photograph of another elastic PnC with a gradually tuned boundary. Here, ξ_x equals from $0.06a$ (at the bottom) to $0.22a$ (at the top). Only four layers of columns are assembled in the PnC on both sides of the boundary. (b) Eigenvalue calculation of the whole PnC. Frequency-separated (red) dots represent elastic resonant modes, appearing at different positions along the boundary. (c) Normalized elastic intensity spectrum of these resonant modes when excited. E_m and E_0 represent the maximal intensity measured in the whole PnC and the intensity measured near the plane-wave source, respectively. (d),(e) Measured and simulated out-of-plane-displacement field distributions of the rainbow resonant modes at different frequencies.

in perfect agreement with the results of the eigenvalue calculations.

Displacement field distributions of the resonant states at different frequencies are measured, as shown in Fig. 4(d) (for all resonant states, see Fig. S7 within the Supplemental Material [36]). The experimental results correspond well with the simulation ones [shown in Fig. 4(e)], validating elastic rainbow concentration. Note that these resonant states' mode volumes are relatively large due to the small frequency separation between adjacent resonant modes in this PnC, i.e., less than 0.5 kHz (about 0.6% relative bandwidth). Each resonance appears as a long grain with multiple wavelengths along the boundary. Although they are not excited by elastic waves propagating along the boundary, they still exhibit an asymmetric energy distribution in the boundary direction. Each resonant state is shaped like a tadpole, exhibiting the strongest energy localization on the side with larger ξ_x.

VI. DIVERSE DESIGN FOR THE ELASTIC RAINBOW CONCENTRATOR

In our elastic rainbow concentrator, the number of resonant states in the boundary is determined by the number of different ξ_x. If the value range of ξ_x is determined, e.g., from $0.06a$ to $0.22a$ in our last experiment, a smaller $\Delta\xi_x$ between each adjacent layer will result in more resonant states over the same fixed frequency range.

Figures 5(a) and 5(b) show two PnCs similar to the one in Fig. 4(a), but there are fewer layers in the boundary direction corresponding to 8 and 16 layers, respectively. $\Delta\xi_x$ between each adjacent layer in the two samples is $0.01a$ and $0.02a$, respectively. According to eigenvalue calculations shown in Figs. 5(c) and 5(d), only 13 and 7 rainbow resonant states exist in the two PnC, respectively. We also calculate that the number of resonance states corresponding to the 10-layer and 20-layer structures is 8 and

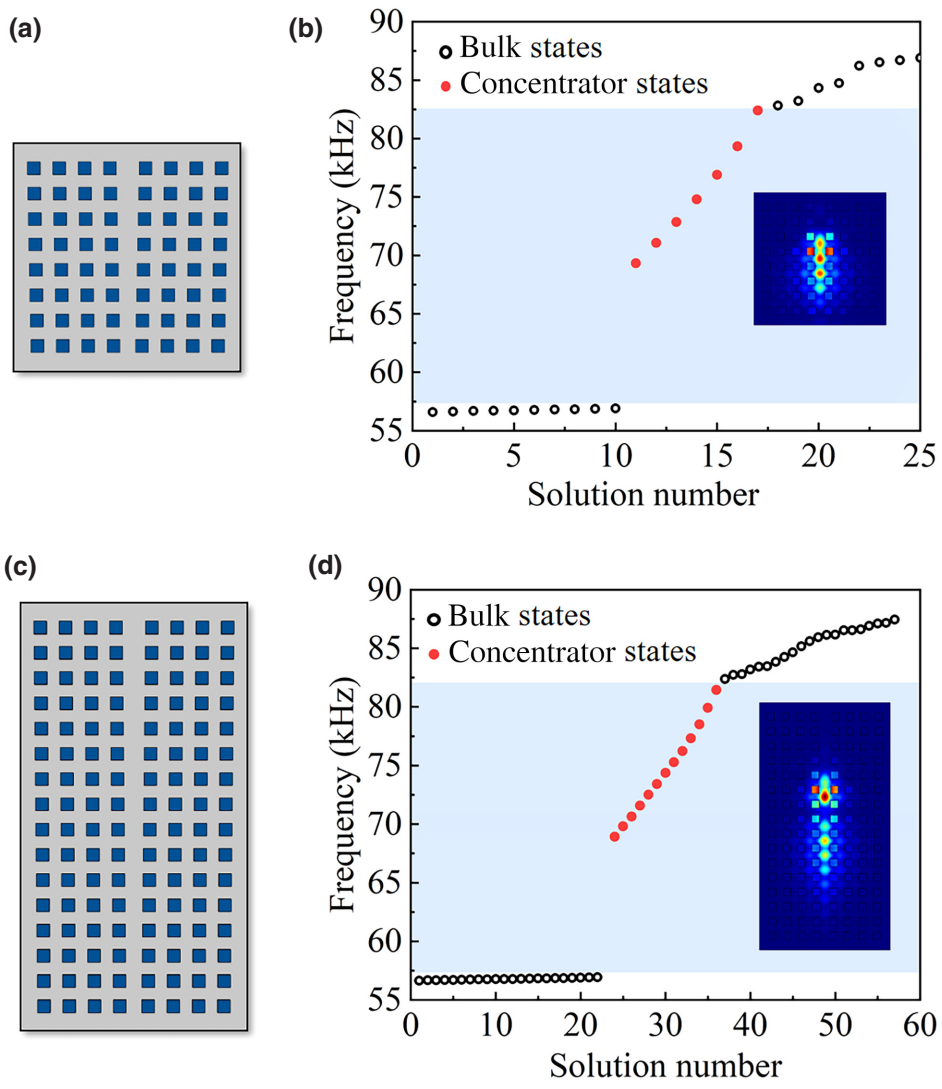

FIG. 5. Configurable rainbow concentrators. (a),(b) PnCs similar to the one in Fig. 4(a) but with fewer layers along the gradually tuned boundary. $\Delta\xi$ between each adjacent layer in the two samples is $0.02a$ and $0.01a$. (c),(d) Eigenvalue calculations of the two PnCs. Insets show simulated out-of-plane-displacement field distributions of the rainbow resonant states, the operating frequencies of which are 74.8 and 73.43 kHz, respectively.

17, respectively. These data are then fitted to obtain the following linear relationship: $C_n = 0.889L_n - 0.695$, where C_n is the number of these states, and L_n is the number of layers along the boundary, as shown in Fig. 7 (see Appendix B).

Displacement field distributions of the resonant states in the two cases are shown in the insets of the figures. As the frequency separation between the resonant states increases, their mode volumes decrease approximately linearly. In the PnC of Fig. 5(a) [Fig. 5(b)], the frequency separation between adjacent resonant states is about 1.76 kHz (0.82 kHz), and their mode volume is only about 1/4 (1/2) of that in Fig. 4(a).

Clearly, by designing different ranges and gradients of ξ_x for the boundary of the PnC, the frequency range, number, and mode volume of the rainbow resonant states can be effectively tuned. It provides a high degree of freedom for elastic wave manipulation and is promising for applications, e.g., acoustofluidics, elastic energy harvesting, and spatial wave switching [13,21].

VII. CONCLUSIONS

This paper verifies a recently proposed exotic wave localization experimentally, i.e., rainbow concentration, exemplarily on an elastic system. We demonstrate that, by bringing a homogeneous dislocation, i.e., a line defect, into a plate PnC, two separated PnCs have distinct Zak phases due to different directional translations, leading to deterministic interface states along with the defect. Different translations can modulate the group velocity of these interface states. Thus, we can achieve rainbow trapping and rainbow concentration for elastic waves. Compared with previous theoretical approaches, the elastic rainbow effect realized by our present method is simple and configurable, not only for design but also for practical sample implementation and miniaturization. This work undoubtedly provides diversity for the precise manipulation of elastic waves in both frequency and spatial domains. It is promising for applications, e.g., nondestructive evaluation [50], wideband energy harvesting [13], and spatial wave switching [21]. Moreover. this method of modulating the boundary states by graded translational deformations can be extended to high-frequency microwave acoustics, e.g., surface acoustic waves, for on-demand storage and extraction of chip-scale phonons used in acoustofluidics [51] and phononic computing [52] and information processing [53].

ACKNOWLEDGMENTS

The work is jointly supported by the National Key R&D Program of China (Grants No. 2021YFB3801801, No. 2017YFA0305100, and No. 2017YFA0303702) and the National Natural Science Foundation of China (Grants No. 11890702, No. 92163133, and No. 51732006). We also acknowledge support from the Fundamental Research Funds for Central Universities. Z.-D.Z. acknowledge the support from the China Postdoctoral Science Foundation (Grant No. 2022M711571).

APPENDIX A: IN-PLANE ELASTIC WAVE RAINBOW TRAPPING

The method for realizing elastic rainbow metamaterials in the main text can achieve a similar effect, as long as there is a complete band gap in the band structure. From the bands in Fig. 1, there is also a complete band gap in the in-plane Lamb mode. Here, it is confirmed by numerical calculation that the in-plane Lamb wave also realizes the rainbow effect in a complete band gap. As shown in Fig. 6(b), the deterministic interface state of the in-plane Lamb waves is a function of the translational vector. The eigenmodes of this interface state show that the in-plane Lamb waves are mainly localized at the boundary. The rainbow localization of the in-plane Lamb waves can also be achieved, as shown in Fig. 6(d).

APPENDIX B: THE RELATIONSHIP BETWEEN THE CONCENTRATION STATE (C_n) AND THE NUMBER OF LAYERS (L_n)

We calculate the number of resonance states corresponding to the 10-layer and 20-layer samples to be 8 and 17. Then, we fit these data, as shown in Fig. 7, and obtain the following linear relationship: $C_n = 0.889L_n - 0.695$.

APPENDIX C: METHODS

1. Numerical simulations

We perform a 3D finite-element simulation using the commercial software COMSOL Multiphysics with the structural mechanics module. The aluminum-alloy-plate density, Young's modulus, and Poisson ratio are 2810 kg m^{-3}, 70.368 GPa, and 0.314, respectively. For the finite-element simulation, meshes are set to $<a/10$ to ensure the accuracy of the calculation. An eigenfrequency study with parameter sweep calculates the PnC's band structure. The frequency-domain study obtains displacement field distributions of the elastic waves.

2. Sample preparation

Using a precision CNC milling machine, we prepare the PnC samples on aluminum-alloy plates with a fixed thickness of about 2.2 cm. The Young's modulus and Poisson ratio of the plates are determined by adopting the ultrasonic scattering-echo method. A 2-inch margin on the plate boundary is left for 3M™ Damping Foil 2552, to reduce unwanted mechanical reflection from the PnC edges during the experiments.

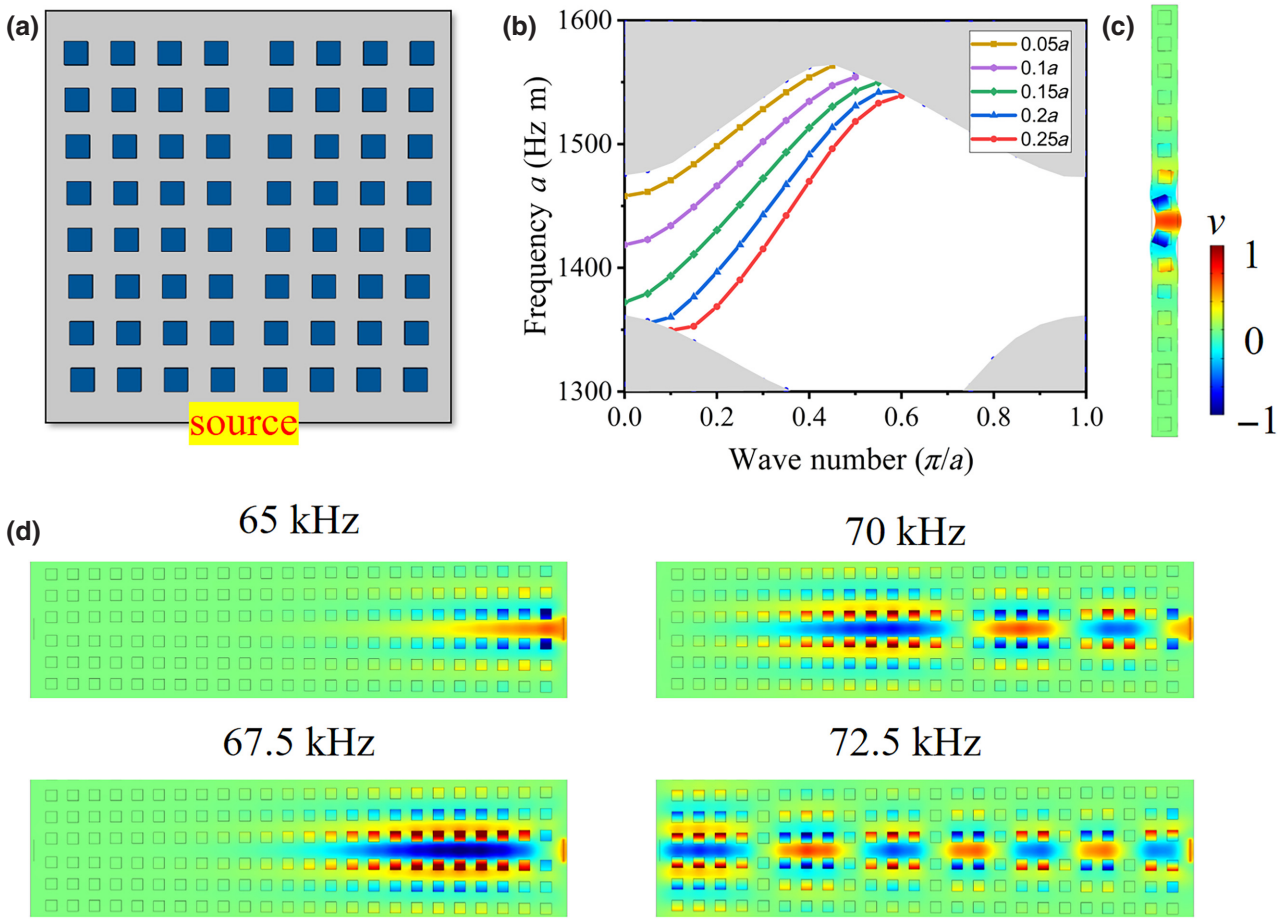

FIG. 6. In-plane elastic wave rainbow trapping. (a) Schematic illustration of elastic rainbow trapping. (b) Dispersion bands of the interface states of supercells. (c) Eigenmodes of deterministic interface states for the in-plane Lamb wave. (d) In-plane-displacement field distributions of interface states corresponding to different frequencies.

3. Experimental measurements

Broadband piezoelectric transducers (centered at 75 kHz) are used as actuators, bonded to the surface of the PnC with 3M™ Scotch-Weld™ structural acrylic adhesives. An arbitrary-wave generator generates alternating signals of tens of kHz, amplified to excite the transducer. A laser Doppler vibrometer is used to record the out-of-plane displacement of the elastic waves, offering a 2D distribution field after scanning.

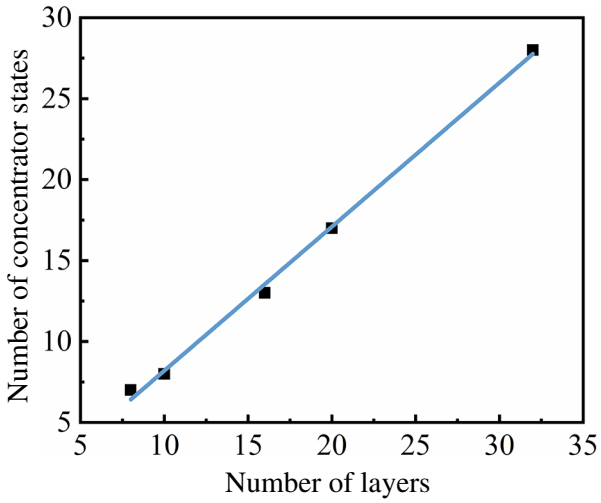

FIG. 7. Relationship between the concentration state (C_n) and the number of layers (L_n).

[1] Y. Xu, Y. Fu, and H. Chen, Planar gradient metamaterials, Nat. Rev. Mater. **1**, 16067 (2016).
[2] Z. Li, M. H. Kim, C. Wang, Z. Han, S. Shrestha, A. C. Overvig, M. Lu, A. Stein, A. M. Agarwal, M. Lončar, and N. Yu, Controlling propagation and coupling of waveguide modes using phase-gradient metasurfaces, Nat. Nanotechnol. **12**, 675 (2017).
[3] L. Lu, J. D. Joannopoulos, and M. Soljačić, Topological photonics, Nat. Photonics **8**, 821 (2014).
[4] S. Cummer, J. Christensen, and A. Alù, Controlling sound with acoustic metamaterials, Nat. Rev. Mater. **1**, 16001 (2016).
[5] Y. F. Wang, Y. Z. Wang, B. Wu, W. Chen, and Y. S. Wang, Tunable and active phononic crystals and metamaterials, Appl. Mech. Rev. **72**, 040801 (2020).

[6] S. D. Huber, Topological mechanics, Nat. Phys. **12**, 621 (2016).

[7] H. Zhu and F. Semperlotti, Anomalous Refraction of Acoustic Guided Waves in Solids with Geometrically Tapered Metasurfaces, Phys. Rev. Lett. **117**, 034302 (2016).

[8] J. M. Kweun, H. J. Lee, J. H. Oh, H. M. Seung, and Y. Y. Kim, Transmodal Fabry-Pérot Resonance: Theory and Realization with Elastic Metamaterials, Phys. Rev. Lett. **118**, 205901 (2017).

[9] Y. Liu, Z. Liang, F. Liu, O. Diba, A. Lamb, and J. Li, Source Illusion Devices for Flexural Lamb Waves Using Elastic Metasurfaces, Phys. Rev. Lett. **119**, 034301 (2017).

[10] Q. Xie, S. Mezil, P. H. Otsuka, M. Tomoda, J. Laurent, O. Matsuda, Z. Shen, and O. B. Wright, Imaging gigahertz zero-group-velocity Lamb waves, Nat. Commun. **10**, 2228 (2019).

[11] A. S. Gliozzi, M. Miniaci, A. Chiappone, A. Bergamini, B. Morin, and E. Descrovi, Tunable photo-responsive elastic metamaterials, Nat. Commun. **11**, 2576 (2020).

[12] G. J. Chaplain, J. M. De Ponti, A. Colombi, R. Fuentes-Dominguez, P. Dryburg, D. Pieris, R. J. Smith, A. Clare, M. Clark, and R. V. Craster, Tailored elastic surface to body wave Umklapp conversion, Nat. Commun. **11**, 3267 (2020).

[13] G. Lee, D. Lee, J. Park, Y. Jang, M. Kim, and J. Rho, Piezoelectric energy harvesting using mechanical metamaterials and phononic crystals, Commun. Phys. **5**, 94 (2022).

[14] X. Fu and T. J. Cui, Recent progress on metamaterials: From effective medium model to real-time information processing system, Prog. Quantum. Electron. **67**, 100223 (2019).

[15] Q. Gan, Y. J. Ding, and F. J. Bartoli, "Rainbow" Trapping and Releasing at Telecommunication Wavelengths, Phys. Rev. Lett. **102**, 056801 (2009).

[16] Q. Gan, Z. Fu, Y. J. Ding, and F. J. Bartoli, Ultrawide-Bandwidth Slow-Light System Based on THz Plasmonic Graded Metallic Grating Structures, Phys. Rev. Lett. **100**, 256803 (2008).

[17] R. J. P. Engelen, D. Mori, T. Baba, and L. Kuipers, Two Regimes of Slow-Light Losses Revealed by Adiabatic Reduction of Group Velocity, Phys. Rev. Lett. **101**, 103901 (2008).

[18] L. Chen, G. P. Wang, Q. Gan, and F. J. Bartoli, Rainbow trapping and releasing by chirped plasmonic waveguides at visible frequencies, Appl. Phys. Lett. **97**, 153115 (2010).

[19] M. S. Jang and H. Atwater, Plasmonic Rainbow Trapping Structures for Light Localization and Spectrum Splitting, Phys. Rev. Lett. **107**, 207401 (2011).

[20] Z. Xu, J. Shi, R. J. Davis, X. Yin, and D. F. Sievenpiper, Rainbow Trapping with Long Oscillation Lifetimes in Gradient Magnetoinductive Metasurfaces, Phys. Rev. Appl. **12**, 024043 (2019).

[21] J. Chen, W. Liang, and Z. Y. Li, Switchable slow light rainbow trapping and releasing in strongly coupling topological photonic systems, Photonics Res. **7**, 1075 (2019).

[22] J. Zhu, Y. Chen, X. Zhu, F. J. Garcia-Vidal, X. Yin, W. Zhang, and X. Zhang, Acoustic rainbow trapping, Sci. Rep. **3**, 1728 (2013).

[23] V. Romero-García, R. Picó, A. Cebrecos, V. J. Sánchez-Morcillo, and K. Staliunas, Enhancement of sound in chirped sonic crystals, Appl. Phys. Lett. **102**, 091906 (2013).

[24] Z. Tian, C. Shen, J. Li, E. Reit, H. Bachman, J. E. S. Socolar, S. A. Cummer, and T. J. Huang, Dispersion tuning and route reconfiguration of acoustic waves in valley topological phononic crystals, Nat. Commun. **11**, 762 (2020).

[25] Z. Tian and L. Yu, Rainbow trapping of ultrasonic guided waves in chirped phononic crystal plates, Sci. Rep. **7**, 40004 (2017).

[26] J. M. De Ponti, L. Iorio, E. Riva, R. Ardito, F. Braghin, and A. Corigliano, Selective Mode Conversion and Rainbow Trapping via Graded Elastic Waveguides, Phys. Rev. Appl. **16**, 034028 (2021).

[27] J. M. De Ponti, A. Colombi, R. Ardito, F. Braghin, A. Corigliano, and R. V. Craster, Graded elastic metasurface for enhanced energy harvesting, New. J. Phys. **22**, 013013 (2020).

[28] J. M. De Ponti, A. Colombi, E. Riva, R. Ardito, F. Braghin, A. Corigliano, and R. V. Craster, Experimental investigation of amplification, via a mechanical delay-line, in a rainbow-based metamaterial for energy harvesting, Appl. Phys. Lett. **117**, 143902 (2020).

[29] L. Cao, Y. Zhu, Y. Xu, S. Fan, Z. Yang, and B. Assouar, Elastic bound state in the continuum with perfect mode conversion, J. Mech. Phys. Solids **154**, 104502 (2021).

[30] M. Alshaqaq, C. Sugino, and A. Erturk, Programmable Rainbow Trapping and Band-Gap Enhancement via Spatial Group-Velocity Tailoring in Elastic Metamaterials, Phys. Rev. Appl. **17**, L021003 (2022).

[31] B. Ungureanu, M. P. Makwana, R. V. Craster, and S. Guenneau, Localizing Elastic Edge Waves via the Topological Rainbow Effect, Phys. Rev. Appl. **15**, 014057 (2021).

[32] G. J. Chaplain, J. M. De Ponti, G. Aguzzi, A. Colombi, and R. V. Craster, Topological Rainbow Trapping for Elastic Energy Harvesting in Graded Su-Schrieffer-Heeger Systems, Phys. Rev. Appl. **14**, 054035 (2020).

[33] Y. Nakata, Y. Ito, Y. Nakamura, and R. Shindou, Topological Boundary Modes from Translational Deformations, Phys. Rev. Lett. **124**, 073901 (2020).

[34] C. Lu, C. Wang, M. Xiao, Z. Q. Zhang, and C. T. Chan, Topological Rainbow Concentrator Based on Synthetic Dimension, Phys. Rev. Lett. **126**, 113902 (2021).

[35] B. Graczykowski, M. Sledzinska, F. Alzina, J. Gomis-Bresco, J. S. Reparaz, M. R. Wagner, and C. M. Sotomayor Torres, Phonon dispersion in hypersonic two-dimensional phononic crystal membranes, Phys. Rev. B **91**, 075414 (2015).

[36] See the Supplemental Material at http://link.aps.org/supplemental/10.1103/PhysRevApplied.18.044015 for details of the polarization index, the quasi-one-dimensional Wannier function, the spectral flow of a localized mode across a bulk frequency gap, the interface state due to the Zak phase being submerged in the bulk state when there is no complete band gap, and the normalized energy-density distributions along the interface.

[37] M. Xiao, Z. Q. Zhang, and C. T. Chan, Surface Impedance and Bulk Band Geometric Phases in One-Dimensional Systems, Phys. Rev. X **4**, 021017 (2014).

[38] M. Xiao, G. Ma, Z. Yang, P. Sheng, Z. Q. Zhang, and C. T. Chan, Geometric phase and band inversion in periodic acoustic systems, Nat. Phys. **11**, 240 (2015).
[39] X. Huang, Y. Yang, Z. H. Hang, Z. Q. Zhang, and C. T. Chan, Geometric phase induced interface states in mutually inverted two-dimensional photonic crystals, Phys. Rev. B **93**, 085415 (2016).
[40] J. Chai, L. Liu, P. Hu, H. Xiang, and D. Han, Interface states and bound states in the continuum in photonic crystals with different lattice constants, Opt. Lett. **45**, 5652 (2020).
[41] Y. Yang, X. Huang, and Z. H. Hang, Experimental Characterization of the Deterministic Interface States in Two-Dimensional Photonic Crystals, Phys. Rev. Applied **5**, 034009 (2016).
[42] X. Huang, M. Xiao, Z. Q. Zhang, and C. T. Chan, Sufficient condition for the existence of interface states in some two-dimensional photonic crystals, Phys. Rev. B **90**, 075423 (2014).
[43] Y. Yang, T. Xu, Y. F. Xu, and Z. H. Hang, Zak phase induced multiband waveguide by two-dimensional photonic crystals, Opt. Lett. **42**, 3085 (2017).
[44] X. D. Chen, W. M. Deng, F. L. Shi, F. L. Zhao, M. Chen, and J. W. Dong, Direct Observation of Corner States in Second-Order Topological Photonic Crystal Slabs, Phys. Rev. Lett. **122**, 233902 (2019).
[45] B. Y. Xie, G. X. Su, H. F. Wang, H. Su, X. P. Shen, P. Zhan, M. H. Lu, Z. L. Wang, and Y. F. Chen, Visualization of Higher-Order Topological Insulating Phases in Two-Dimensional Dielectric Photonic Crystals, Phys. Rev. Lett. **122**, 233903 (2019).
[46] G. Wang, Z. Zhang, Y. Gu, D. Liao, Y. Cheng, and X. Liu, Zak-phase-inspired acoustic topological edge states on the honeycomb lattice, Phys. Rev. B **103**, 094102 (2021).
[47] L. L. Lin and Z. Y. Li, Interface states in photonic crystal heterostructures, Phys. Rev. B **63**, 033310 (2001).
[48] J. A. Schuller, E. S. Barnard, W. Cai, Y. C. Jun, J. S. White, and M. L. Brongersma, Plasmonics for extreme light concentration and manipulation, Nat. Mater. **9**, 193 (2010).
[49] C. Li, L. Xu, L. Zhu, S. Zou, Q. H. Liu, Z. Wang, and H. Chen, Concentrators for Water Waves, Phys. Rev. Lett. **121**, 104501 (2018).
[50] I. Solodov, J. Bai, S. Bekgulyan, and G. Busse, A local defect resonance to enhance acoustic wave-defect interaction in ultrasonic nondestructive evaluation, Appl. Phys. Lett. **99**, 211911 (2011).
[51] Z. Ni, G. Xu, J. Huang, G. Yao, J. Tu, X. Guo, and D. Zhang, Lamb wave coupled resonance for SAW acoustofluidics, Appl. Phys. Lett. **118**, 051103 (2021).
[52] M. Merklein, B. Stiller, K. Vu, S. J. Madden, and B. J. Eggleton, A chip-integrated coherent photonic-phononic memory, Nat. Commun. **8**, 574 (2017).
[53] H. Shin, J. A. Cox, R. Jarecki, A. Starbuck, Z. Wang, and P. T. Rakich, Control of coherent information via on-chip photonic–phononic emitter–receivers, Nat. Commun. **6**, 6427 (2015).